Supersymmetric Signal Analysis and Mass Reconstruction of the Chargino ($\widetilde{\chi}_1^{\pm}$) at the International Linear Collider

Kevin Fiedler
High Energy Physics
University of Colorado

April 11, 2011

Thesis Committee

Dr. Uriel Nauenberg (Advisor)
University of Colorado at Boulder - Department of Physics

Dr. John Cumalat (Honors Representative)
University of Colorado at Boulder - Department of Physics

Dr. Alexander Gorokhovsky
University of Colorado at Boulder - Department of Mathematics

Abstract

The hadronic decay modes of the light chargino, $\widetilde{\chi}_1^{\pm}$, are examined at several parameter points. With the 500 GeV International Linear Collider, the signal is reconstructed and analyzed in the presence of Standard Model background with 100 fb^{-1} and 250 fb^{-1} of data. Once the signal has been analyzed and the Standard Model background removed, three mass measurement techniques are investigated. Finally, the masses of the $\widetilde{\chi}_1^{\pm}$ and $\widetilde{\chi}_1^0$ are measured to within 2% of the known value.

Contents

List of Tables

List of Figures

1 Introduction and Background

1.1 The Standard Model and Supersymmetry

The Standard Model of particle physics, proposed in the 1970's, is the most complete and well-tested physical theory of elementary particle physics. It makes many experimental claims which have been confirmed to better than 1%. Threrefore, the Standard Model is quite successful in almost all areas.

Despite this success, there is a major failing of the Standard Model, outside of the lack of gravitational interactions in the theory. The Standard Model predicts that the mass of the Higgs boson, the boson that gives mass to all particles, diverges quadratically with energy. This divergence is also known as the hierarchy problem.

One possible theory for physics beyond the Standard Model that solves the hierarchy problem is supersymmetry (SUSY) [1]. SUSY postulates the existence of a superpartner for every known particle. These heavy, unstable superpartners are called sparticles. Sparticles have a profound influence on the hierarchy problem the Standard Model is currently grappling with. With the inclusion of the sparticles, the mass of the Higgs boson no longer diverges quadratically, due to cancellations in the loop diagrams. There are several other arguments in favor of SUSY. Without the additions of supersymmetry, the convergence of the strong, weak, and electromagnetic coupling constants is close, but not exact near the energy of the Big Bang. By including the sparticles introduced by supersymmetry, the coupling constants converge to a single value at high energies. Secondly, SUSY provides a natural candidate for dark matter: the lightest supersymmetric particle (LSP). The LSP cannot decay to a lighter Standard Model particle due to the conservation of a quantum number called R-parity which is 1 for all Standard Model particles and -1 for sparticles. Consequently, the LSP is stable and fulfills all the requirements for dark matter.

1.2 The International Linear Collider and the Silicon Based Detector

Currently, the search for SUSY is centered on the Large Hadron Collider (LHC) in Geneva, Switzerland. However, the focus of this study will be on the proposed successor to the LHC: the International Linear Collider (ILC). The ILC's design specifications [2] detail a linear geometry with a center of mass

collision energy of 500 GeV for the e^+e^- beams. A linear collider geometry is necessary for e^+e^- initial states because circular accelerator geometries lose too much energy due to synchrotron radiation. In addition, e^+e^- initial states provide a cleaner signal than hadronic states due to a more precise determination of the initial energies and momenta. Hence, a more precise determination of the sparticle properties can be obtained with the ILC than with the LHC.

Within the collider itself, the detector records decays produced from the interaction. Currently, two detector concepts have been approved by the International Detector Advisory Group (IDAG): Silicon Detector (SiD) [3] and International Linear Detector (ILD) [4]. SiD is a collaboration that supports a silicon based detector that will determine the energies and momenta of the particles produced in the collisions. The research group led by Professor Uriel Nauenberg is part of the SiD collaboration and focuses on the BeamCal, which is in the far forward region. The BeamCal occupies the region directly around the beampipe out to the endcaps. Its goal is to provide greater detection capabilities at small polar angles and the ability to make crucial benchmarking measurements feasible.

1.3 mSUGRA Parameter Points

There are several competing theories that are subsets of supersymmetry. One of particular interest is minimal supergravity (mSUGRA) [1]. This model is not completely general, as it assumes a particular symmetry breaking mechanism. However, it reduces a very large parameter space to only five parameters. These are: m_0, $m_{1/2}$, A_0, $\tan(\beta)$, and $\text{sign}(\mu)$, which are the scalar mass, spin-1/2 mass, trilinear coupling, ratio of the higgs doublets, and the sign of the quadratic term in the superpotential, respectively.

There are a series of benchmarks detailed in [5], and updated in [6] to include the WMAP (Wilkinson Microwave Anisotropy Probe) constraints, for the many possible scenarios at the ILC. Since this study is focused on reconstructing the mass of the light chargino ($\widetilde{\chi}_1^{\pm}$), only the parameter points where the $\widetilde{\chi}_1^{\pm}$ is kinematically accessible will be studied. In particular, there are only two such points at 500 GeV, E' and B', detailed in those papers.

Additionally, there is a set of benchmarks designed specifically for the ILC [5]. Within these benchmarks there is another parameter point of interest, α. Consequently, the $\widetilde{\chi}_1^{\pm}$ will be analyzed at all three of these parameter points.

Parameter Point E'

The mSUGRA parameters for the point E' are:

m_0	1530
$m_{1/2}$	300
$\tan(\beta)$	10
$\mathrm{sgn}(\mu)$	1
A_0	0

Table 1: mSUGRA Parameters at Point E'

Additionally, the masses associated with this point, calculated by SPheno [7] are given by:

Particle	Mass(GeV)	Particle	Mass (GeV)
W^+	8.040x10^1	$\widetilde{e}_L^-$	1.538x10^3
h^0	1.156x10^2	$\widetilde{e}_R^-$	1.533x10^3
H^0	1.592x10^3	$\widetilde{\nu}_e$	1.535x10^3
A^0	1.592x10^3	$\widetilde{\mu}_L^-$	1.538x10^3
H^+	1.594x10^3	$\widetilde{\mu}_R^-$	1.533x10^3
$\widetilde{d}_L$	1.635x10^3	$\widetilde{\nu}_\mu$	1.535x10^3
$\widetilde{d}_R$	1.629x10^3	$\widetilde{\tau}_1^-$	1.519x10^3
$\widetilde{u}_L$	1.633x10^3	$\widetilde{\tau}_2^-$	1.532x10^3
$\widetilde{u}_R$	1.628x10^3	$\widetilde{\nu}_\tau$	1.529x10^3
$\widetilde{s}_L$	1.635x10^3	$\widetilde{g}$	7.801x10^2
$\widetilde{s}_R$	1.629x10^3	$\widetilde{\chi}_1^0$	1.233x10^2
$\widetilde{c}_L$	1.633x10^3	$\widetilde{\chi}_2^0$	2.364x10^2
$\widetilde{c}_R$	1.628x10^3	$\widetilde{\chi}_3^0$	$-$4.934x10^2
$\widetilde{b}_1$	1.342x10^3	$\widetilde{\chi}_4^0$	5.065x10^2
$\widetilde{b}_2$	1.616x10^3	$\widetilde{\chi}_1^+$	2.364x10^2
$\widetilde{t}_1$	9.856x10^2	$\widetilde{\chi}_2^+$	5.072x10^2
$\widetilde{t}_2$	1.352x10^3		

Table 2: SUSY Particle Masses at Point E'. The mass of the $\widetilde{\chi}_3^0$ is negative in the table. This results from the spectrum calculation and is partly a sign convention. However, the actual mass of the physical particle is positive. Additionally, natural units are used throughout this analysis. This means that $c = 1$ and so energy, mass, and momentum all have units of GeV. It should be clear from the context which variable is being considered.

As can be seen above, the mass difference between the $\widetilde{\chi}_1^0$ and $\widetilde{\chi}_1^\pm$ is approximately 113 GeV. Additionally, the very large value of m_0 causes the slepton masses to be very large; many of which are greater than 1 TeV. Since this mass difference is greater than the mass of the W boson and the sleptons are so heavy, the $\widetilde{\chi}_1^\pm$ will decay exclusively through the following decay channel:

$$\widetilde{\chi}_1^\pm \rightarrow \widetilde{\chi}_1^0 W^\pm \tag{1}$$

The cross section, in units of femtobarns (fb), governs how often the event of interest is produced. The total number of events for a given luminosity,

with units of fb^{-1}, is simply the product of the cross section and the luminosity. The cross sections for this parameter point are displayed below.

SUSY Process	Cross Section (fb)
$e^+e^- \to \widetilde{\chi}_1^0\widetilde{\chi}_1^0$	$2.34\text{x}10^{0}$
$e^+e^- \to \widetilde{\chi}_1^0\widetilde{\chi}_2^0$	$1.06\text{x}10^{-1}$
$e^+e^- \to \widetilde{\chi}_2^0\widetilde{\chi}_2^0$	$7.03\text{x}10^{-3}$
$e^+e^- \to \widetilde{\chi}_1^+\widetilde{\chi}_1^-$	$6.10\text{x}10^{1}$
$e^+e^- \to h^0Z^0$	$6.44\text{x}10^{1}$

Table 3: Cross Sections at Point E'

Parameter Point B'

The mSUGRA parameters for the point B' are:

m_0	60
$m_{1/2}$	250
$\tan(\beta)$	10
$\text{sgn}(\mu)$	1
A_0	0

Table 4: mSUGRA Parameters at Point B'

Once again, the masses associated with this point, calculated by SPheno [7] are given by:

Particle	Mass (GeV)	Particle	Mass (GeV)
W^+	8.040x10^1	$\widetilde{e}_L^-$	1.862x10^2
h^0	1.101x10^2	$\widetilde{e}_R^-$	1.200x10^2
H^0	3.777x10^2	$\widetilde{\nu}_e$	1.684x10^2
A^0	3.773x10^2	$\widetilde{\mu}_L^-$	1.862x10^2
H^+	3.861x10^2	$\widetilde{\mu}_R^-$	1.199x10^2
$\widetilde{d}_L$	5.650x10^2	$\widetilde{\nu}_\mu$	1.684x10^2
$\widetilde{d}_R$	5.420x10^2	$\widetilde{\tau}_1^-$	1.106x10^2
$\widetilde{u}_L$	5.595x10^2	$\widetilde{\tau}_2^-$	1.903x10^2
$\widetilde{u}_R$	5.422x10^2	$\widetilde{\nu}_\tau$	1.678x10^2
$\widetilde{s}_L$	5.650x10^2	$\widetilde{g}$	6.034x10^2
$\widetilde{s}_R$	5.420x10^2	$\widetilde{\chi}_1^0$	9.651x10^1
$\widetilde{c}_L$	5.595x10^2	$\widetilde{\chi}_2^0$	1.786x10^2
$\widetilde{c}_R$	5.422x10^2	$\widetilde{\chi}_3^0$	$-$3.483x10^2
$\widetilde{b}_1$	5.142x10^2	$\widetilde{\chi}_4^0$	3.675x10^2
$\widetilde{b}_2$	5.424x10^2	$\widetilde{\chi}_1^+$	1.781x10^2
$\widetilde{t}_1$	4.101x10^2	$\widetilde{\chi}_2^+$	3.685x10^2
$\widetilde{t}_2$	5.833x10^2		

Table 5: SUSY Particle Masses at Point B'. The mass of the $\widetilde{\chi}_3^0$ is negative in the table. This results from the spectrum calculation and is partly a sign convention. However, the actual mass of the physical particle is positive. Additionally, natural units are used throughout this analysis. This means that $c = 1$ and so energy, mass, and momentum all have units of GeV. It should be clear from the context which variable is being considered.

In this instance, the mass difference between the $\widetilde{\chi}_1^0$ and the $\widetilde{\chi}_1^\pm$ is approximately 81.5 GeV. Consequently, the decay considered for E' (1) is highly suppressed due to a lack of available phase space. This follows from the fact that the mass of the W boson is very close to the mass difference between the $\widetilde{\chi}_1^0$ and the $\widetilde{\chi}_1^\pm$. Instead, the primary modes of $\widetilde{\chi}_1^\pm$ decay are to $\widetilde{\tau}_1^\pm$ and $\widetilde{\nu}_\tau$. In fact, the following two decays comprise almost 70 % of $\widetilde{\chi}_1^\pm$ decays.

$$\widetilde{\chi}_1^\pm \rightarrow \widetilde{\tau}_1^\pm \nu_\tau \tag{2}$$

$$\widetilde{\chi}_1^\pm \rightarrow \widetilde{\nu}_\tau \tau^\pm \tag{3}$$

The cross sections for this parameter point are:

SUSY Process	Cross Section (fb)
$e^+e^- \to \widetilde{e}_R^-\widetilde{e}_R^+$	8.27x10^2
$e^+e^- \to \widetilde{e}_R^-\widetilde{e}_L^+$	2.58x10^1
$e^+e^- \to \widetilde{e}_L^-\widetilde{e}_R^+$	1.25x10^2
$e^+e^- \to \widetilde{e}_L^-\widetilde{e}_L^+$	2.60x10^1
$e^+e^- \to \widetilde{\mu}_R^-\widetilde{\mu}_R^+$	2.97x10^2
$e^+e^- \to \widetilde{\mu}_R^-\widetilde{\mu}_L^+$	2.00x10^{-2}
$e^+e^- \to \widetilde{\mu}_L^-\widetilde{\mu}_R^+$	2.00x10^{-2}
$e^+e^- \to \widetilde{\mu}_L^-\widetilde{\mu}_L^+$	4.03x10^1
$e^+e^- \to \widetilde{\tau}_1^-\widetilde{\tau}_1^+$	2.95x10^2
$e^+e^- \to \widetilde{\tau}_1^-\widetilde{\tau}_2^+$	4.13x10^0
$e^+e^- \to \widetilde{\tau}_2^-\widetilde{\tau}_1^+$	4.13x10^0
$e^+e^- \to \widetilde{\tau}_2^-\widetilde{\tau}_2^+$	4.08x10^1
$e^+e^- \to \widetilde{\nu}_e\overline{\widetilde{\nu}}_e$	1.24x10^2
$e^+e^- \to \widetilde{\nu}_\mu\overline{\widetilde{\nu}}_\mu$	5.04x10^1
$e^+e^- \to \widetilde{\nu}_\tau\overline{\widetilde{\nu}}_\tau$	5.08x10^1
$e^+e^- \to \widetilde{\chi}_1^0\widetilde{\chi}_1^0$	7.00x10^2
$e^+e^- \to \widetilde{\chi}_1^0\widetilde{\chi}_2^0$	2.97x10^1
$e^+e^- \to \widetilde{\chi}_1^0\widetilde{\chi}_3^0$	2.96x10^1
$e^+e^- \to \widetilde{\chi}_1^0\widetilde{\chi}_4^0$	6.47x10^0
$e^+e^- \to \widetilde{\chi}_2^0\widetilde{\chi}_2^0$	1.26x10^1
$e^+e^- \to \widetilde{\chi}_1^+\widetilde{\chi}_1^-$	2.96x10^1
$e^+e^- \to h^0Z^0$	6.53x10^1
$e^+e^- \to H^0Z^0$	2.02x10^{-3}

Table 6: Cross Sections at Point B'

Parameter Point α

The mSUGRA parameters for the point α are:

m_0	206
$m_{1/2}$	293
$\tan(\beta)$	10
$\text{sgn}(\mu)$	1
A_0	0

Table 7: mSUGRA Parameters at Point α

The masses associated with the point α, calculated by SPheno [7] are given by:

Particle	Mass (GeV)	Particle	Mass (GeV)
W^+	8.040x10^1	$\widetilde{e}_L^-$	2.892x10^2
h^0	1.117x10^2	$\widetilde{e}_R^-$	2.374x10^2
H^0	4.806x10^2	$\widetilde{\nu}_e$	2.779x10^2
A^0	4.803x10^2	$\widetilde{\mu}_L^-$	2.892x10^2
H^+	4.873x10^2	$\widetilde{\mu}_R^-$	2.373x10^2
$\widetilde{d}_L$	6.790x10^2	$\widetilde{\nu}_\mu$	2.779x10^2
$\widetilde{d}_R$	6.538x10^2	$\widetilde{\tau}_1^-$	2.310x10^2
$\widetilde{u}_L$	6.745x10^2	$\widetilde{\tau}_2^-$	2.912x10^2
$\widetilde{u}_R$	6.546x10^2	$\widetilde{\nu}_\tau$	2.768x10^2
$\widetilde{s}_L$	6.790x10^2	$\widetilde{g}$	7.029x10^2
$\widetilde{s}_R$	6.538x10^2	$\widetilde{\chi}_1^0$	1.156x10^2
$\widetilde{c}_L$	6.745x10^2	$\widetilde{\chi}_2^0$	2.158x10^2
$\widetilde{c}_R$	6.546x10^2	$\widetilde{\chi}_3^0$	$-$4.027x10^2
$\widetilde{b}_1$	6.139x10^2	$\widetilde{\chi}_4^0$	4.203x10^2
$\widetilde{b}_2$	6.523x10^2	$\widetilde{\chi}_1^+$	2.155x10^2
$\widetilde{t}_1$	4.942x10^2	$\widetilde{\chi}_2^+$	4.211x10^2
$\widetilde{t}_2$	6.731x10^2		

Table 8: SUSY Particle Masses at Point α. The mass of the $\widetilde{\chi}_3^0$ is negative in the table. This results from the spectrum calculation and is partly a sign convention. However, the actual mass of the physical particle is positive. Additionally, natural units are used throughout this analysis. This means that $c = 1$ and so energy, mass, and momentum all have units of GeV. It should be clear from the context which variable is being considered.

For this point, the mass difference between the $\widetilde{\chi}_1^0$ and the $\widetilde{\chi}_1^\pm$ is sufficiently large (100 GeV) that the primary decay will be the same as for E' (1). However, due to the larger number of kinematically accessible processes, the same channel has a lower cross section. The cross section are listed below.

SUSY Process	Cross Section (fb)
$e^+e^- \rightarrow \widetilde{e}_R^-\widetilde{e}_R^+$	3.18x10^1
$e^+e^- \rightarrow \widetilde{\mu}_R^-\widetilde{\mu}_R^+$	1.36x10^1
$e^+e^- \rightarrow \widetilde{\tau}_1^-\widetilde{\tau}_1^+$	2.33x10^1
$e^+e^- \rightarrow \widetilde{\chi}_1^0\widetilde{\chi}_1^0$	3.70x10^2
$e^+e^- \rightarrow \widetilde{\chi}_1^0\widetilde{\chi}_2^0$	9.84x10^0
$e^+e^- \rightarrow \widetilde{\chi}_2^0\widetilde{\chi}_2^0$	2.82x10^0
$e^+e^- \rightarrow \widetilde{\chi}_1^+\widetilde{\chi}_1^-$	1.19x10^1
$e^+e^- \rightarrow h^0Z^0$	6.51x10^1

Table 9: Cross Sections at Point α

2 Data Generation and Detector Simulation

Now that several parameter points have been identified, Monte Carlo simulation [8] will be used to study them. Using pseudorandom numbers, events are generated that are representative of the Standard Model background processes as well as the SUSY signal itself. Once this has been accomplished, the ability to disentangle the SUSY signal from the Standard Model background will be examined. For this study, the e^- polarization will be 0.8 (80% right-handed) and the e^+ polarization will be -0.3 (30% left-handed). These polarizations were chosen because they maximize the SUSY cross section while still being within the mechanical constraint of the collider. Additionally, for the initial analysis 100 fb^{-1} of data was generated which was expanded to 250 fb^{-1}.

2.1 Standard Model Background

Event Generation

The Standard Model background is composed of the Standard Model processes thought to be significant at a center of mass energy of 500 GeV at the ILC. The following table contains cross sections for the processes. The number of events generated for each process can then be calculated by multiplying the cross section by the luminosity in units of fb^{-1}. For all processes, except $e^-\gamma$*, $e^+\gamma$*, and two photon, the cross sections were calculated using PYTHIA 6.4 [9]. This was done by generating a small

number of events (typically 10,000) and then extracting the cross section from the output. For the virtual photon processes, $e^-\gamma^*$, $e^+\gamma^*$, and two photon, BDK [10] was used instead of PYTHIA because PYTHIA misestimated the cross section in these cases.

Name	Process	Cross Section (fb)
Z^0 Pair Production	$e^+e^- \to Z^0Z^0$	5.60x10^2
Z^0 Production	$e^+e^- \to Z^0\gamma^*$	1.75x10^4
W Pair Production	$e^+e^- \to W^+W^-$	1.93x10^4
$e^-\gamma^*$ Production	$e^+e^- \to \gamma^*e^-$	1.94x10^6
$e^+\gamma^*$ Production	$e^+e^- \to e^+\gamma^*$	1.94x10^6
Two Photon Events	$e^+e^- \to \gamma^*\gamma^*$	5.47x10^6
Bhabha Scattering†	$e^+e^- \to f\bar{f}$	2.73x10^8

Table 10: Standard Model Background Process List with Cross Sections. Final state fermions $(e, \mu, \tau, u, d, s, c, b, t)$ are specified by f and their antiparticles by $\bar{f}$.
† Not all events in the Bhabha cross section were generated due to the extreme size of the requisite data set and the ease of removal through basic kinematic cuts.

Detector Simulation

Once the events have been generated, the interactions of each event with the detector must be incorporated. For this study, fast reconstruction has been performed with a modified version of MCFast from the org.lcsim analysis framework [11]. Originally, MCFast does not account for any efficiency in the region of the BeamCal, which resides in the far-forward region. However, efficiency tables have been constructed by members of the Nauenberg group [12] that detail the ability of the BeamCal to see an electron with a given energy and momentum vector. This increased visibility is key to the removal of many Standard Model background processes. As a result, MCFast has been extended to include this additional capability. Additionally, a driver that reconstructs jets has been added so that each data file has a list of jets in addition to the list of reconstructed particles. This jet-finding driver uses the JADE jet finding algorithm as in [13] with $y_{cut} = 0.05$. This parameter determines how the jet-finding algorithm rejects potential jets by setting a

cutoff mass from y_{cut}. Once the data has been run through MCFast, it is ready to be analyzed in a signal analysis.

2.2 SUSY Signal

Data generation for the SUSY signal is quite similar to the Standard Model generation process. However, there is one significant difference for the SUSY signal, which is the calculation of the spectrum.

Spectrum Calculation, Event Generation, and Detector Simulation

The spectrum is the relevant masses, cross sections and branching ratios for a SUSY parameter point. This is crucial for the event generation process because PYTHIA does not have the requisite information to generate SUSY data without the spectrum. As such, the program SPheno 2.2.3 (Supersymmetric Phenomenology) [7] is used. Once the spectrum has been calculated, this information is passed to PYTHIA. Then event generation and detector simulation proceed as detailed above.

3 Analysis

To begin the analysis, the Monte Carlo signal is analyzed. It provides verification that the cuts are not distorting the signal too heavily and will be used later in calibrating the mass measurement techniques presented in the Appendices. Then, the signal will be examined using reconstructed particles with the cuts to demonstrate the value in expanding the dataset from 100 fb^{-1} to 250 fb^{-1}. Finally, the Standard Model background will be included to simulate the actual signal of supersymmetry and the Standard Model combined.

3.1 Monte Carlo Particles

With Monte Carlo data, the exact signal that is to be reconstructed can be found. This follows because with Monte Carlo particles, all information about the event is present, which is not the case with reconstructed particles. Therefore, for each parameter point, the $\widetilde{\chi}_1^{\pm}$ signal will be extracted. To do this, only W bosons whose parent was a $\widetilde{\chi}_1^{\pm}$ are selected. Additionally,

both the 100 fb^{-1} and 250 fb^{-1} Monte Carlo particles are presented as a comparison tool.

Parameter Point E'

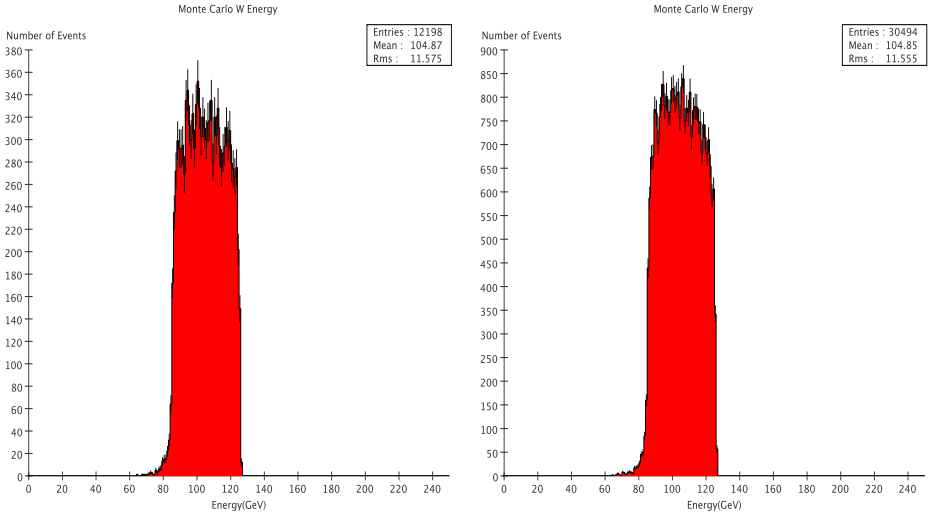

Figure 1: These plots show the Monte Carlo signal after restricting our attention to W bosons from $\widetilde{\chi}_1^{\pm}$ pair production. The 100 fb^{-1} plot is on the left and the 250 fb^{-1} one is on the right. As expected, there is an increase of approximately 2.5 in the number of events.

Parameter Point B'

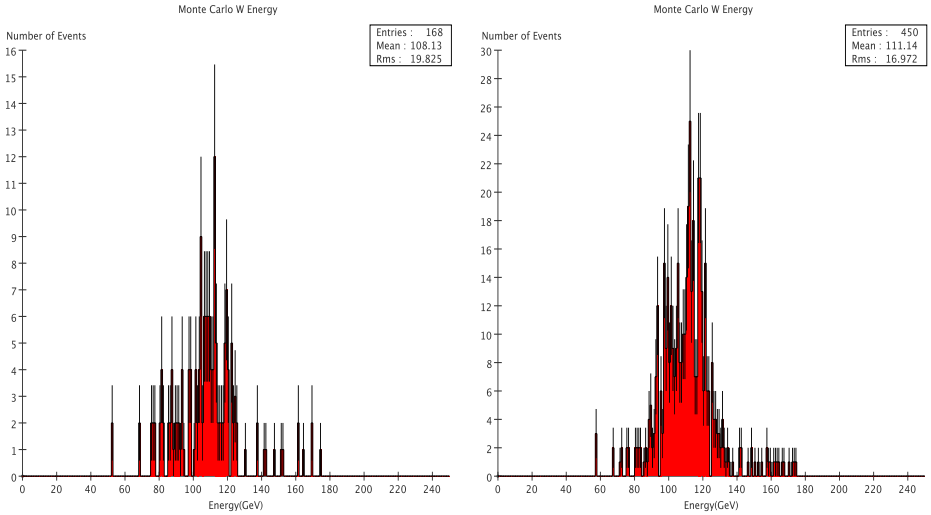

Figure 2: These plots show the Monte Carlo signal after restricting our attention to W bosons from $\widetilde{\chi}_1^{\pm}$ pair production. The 100 fb^{-1} plot is on the left and the 250 fb^{-1} one is on the right. As expected, there is an increase of approximately 2.5 in the number of events. As mentioned previously, this decay is highly suppressed due to lack of available phase space. Therefore, no purely hadronic analysis is possible for this channel at this parameter point.

Parameter Point α

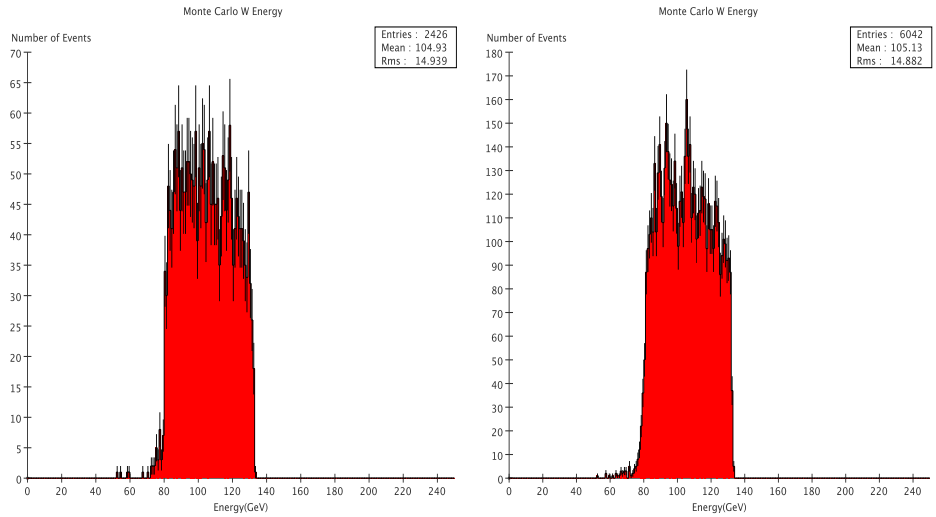

Figure 3: These plots show the Monte Carlo signal after restricting our attention to W bosons from $\widetilde{\chi}_1^{\pm}$ pair production. The 100 fb^{-1} plot is on the left and the 250 fb^{-1} one is on the right. As expected, there is an increase of approximately 2.5 in the number of events.

3.2 Signal Reconstructed Particles

Now that the ideal Monte Carlo signal has been identified, it is possible to determine the reconstructed signal without any background. This will be the signal that is the most realistic view of how the detector would view the SUSY process without the obscuring Standard Model processes. The ideal cuts would remove all the Standard Model background while retaining all the SUSY signal. While this is clearly not feasible, the cuts will be selected so as to remove as many Standard Model events as possible while removing as few SUSY events as possible. The main feature of SUSY signals that will be exploited here is the fact that there is a large amount of missing energy in any SUSY event. Because the $\widetilde{\chi}_1^0$ does not interact with the detector, any SUSY process will have a significant amount of missing energy.

The cuts that have been applied to both the signal and background are listed below. They have been applied to both parameter points E' and α

because the exact nature of supersymmetry is not known beforehand. Point B' does not have enough signal events to proceed with a hadronic analysis. Both scenarios will be investigated to verify that the cuts have not been tuned to detect the $\widetilde{\chi}_1^{\pm}$ at a single parameter point. For each event to be considered a signal event, it must conform to the following:

- Exactly 4 jets as reconstructed with the JADE Jet finding algorithm [11] with the parameter $y_{cut} = 0.05$. These 4 jets must be able to be combined into 2 W bosons with a mass of 75 GeV $< m_W <$ 85 GeV.
- The total visible energy in the event must be less than 350 GeV.
- Each W boson must have less than 175 GeV of energy.
- The angle between the momentum of the two W bosons must be greater than 30 degrees and less than 150 degrees.
- The acoplanarity between the two W bosons must be greater than 10 degrees and less than 170 degrees. Acoplanarity is defined as the angle between the particles when their momentum is projected into the plane perpendicular to the beam axis.

Parameter Point E'

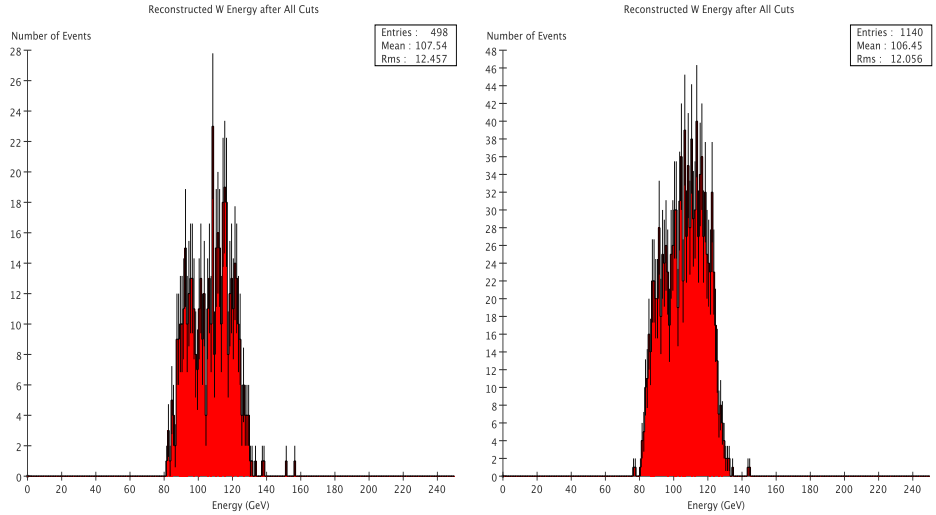

Figure 4: These plots show the just the reconstructed signal after imposing the above cuts. For this plot, no Standard Model processes have been included. The 100 fb^{-1} plot is on the left and the 250 fb^{-1} one is on the right.

Parameter Point α

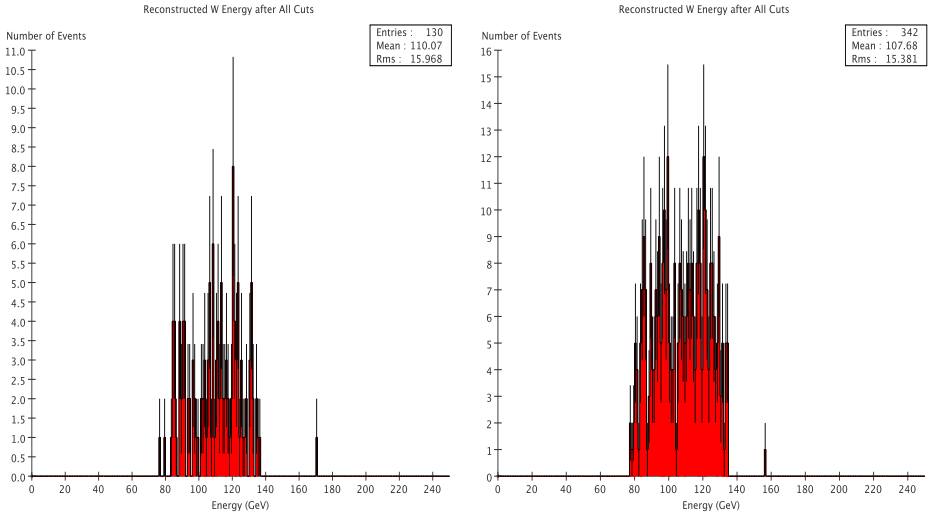

Figure 5: These plots show the just the reconstructed signal after imposing the above cuts. For this plot, no Standard Model processes have been included. The 100 fb^{-1} plot is on the left and the 250 fb^{-1} one is on the right. Event though point α has more signal events than point B', after the cuts necessary to remove the Standard Model background there are not enough signal events to reliably extract a mass.

While each plot at both parameter points has the same general shape as the respective Monte Carlo histograms, the number of events is drastically reduced. While this is partly due to the cuts, the majority of the decrease stems from the jet reconstruction process. Even with the standard jet finding algorithm, it does not produce the expected number of jets for hadronic W boson decays very frequently. This causes the signal to have very low statistics and necessitates the increase to 250 fb^{-1} of data. This also requires a very efficient veto of the Standard Model background. Even with this increase in the amount of available data, the only parameter point where a mass can be extracted is E'.

3.3 Standard Model Background

Parameter Point E'

Now these same cuts will be applied to the Standard Model background data. The major background in this instance is from W boson pair production because it has the same general structure as the SUSY signal. However, most of the background can be removed due to the fact that it does not have enough missing energy. Since only hadronic decays are considered, the missing energy from neutrinos does not mimic the missing energy from $\widetilde{\chi}_1^0$. The cuts will be applied in the same order that they were presented above.

Four Jets with Two W Bosons Cut

The first cut is the most important one from a conceptual perspective. There are many possible decay products for the W bosons produced from the $\widetilde{\chi}_1^{\pm}$. For this analysis, only hadronic final states are being considered. If a W boson decays hadronically, then it will produce two jets. A jet is a set of hadrons which are produced from the hadronization of a quark or gluon. Typically, these particles will be produced in a fairly small cone. Therefore, if there are two W bosons in the event, and they both decayed hadronically, there must be four visible jets. This has advantages over leptonic final states because there are less possible sources of missing energy and momentum from the Standard Model background.

Additionally, these four jets can be recombined to form W bosons, if they were produced from W bosons initially and there is not too much missing energy. As a result, the different possible combinations of pairing jets are investigated until both W bosons have a mass between 75 GeV and 85 GeV. With this restriction in place, the signal and background have the following energy distribution.

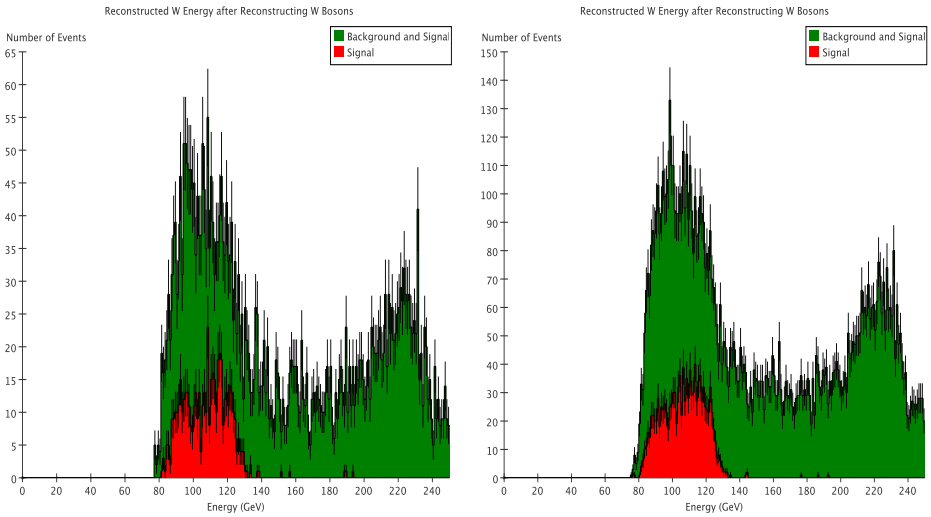

Figure 6: Reconstructed W Boson Energy at Point E' after W Mass Cut. The plot on the left is for 100 fb^{-1} of data and the one on the right is 250 fb^{-1} of data. This plot shows that considering hadronic final states reduces a significant portion of the Standard Model background. To produce this plot, the jets were reconstructed into W bosons with a mass between 75 GeV and 85 GeV.

Total Visible Energy Cut

The next cut that will be applied to this signal is that the total visible energy in the event must be less than 350 GeV. This is an assumption that the mass of the $\widetilde{\chi}_1^0$ is at least 75 GeV so that the total missing energy in any SUSY event is at least 150 GeV. However, this assumption is reasonable as all parameter points considered have $\widetilde{\chi}_1^0$ masses greater than this. For Standard Model events that decay hadronically, the energy losses should be relatively minor.

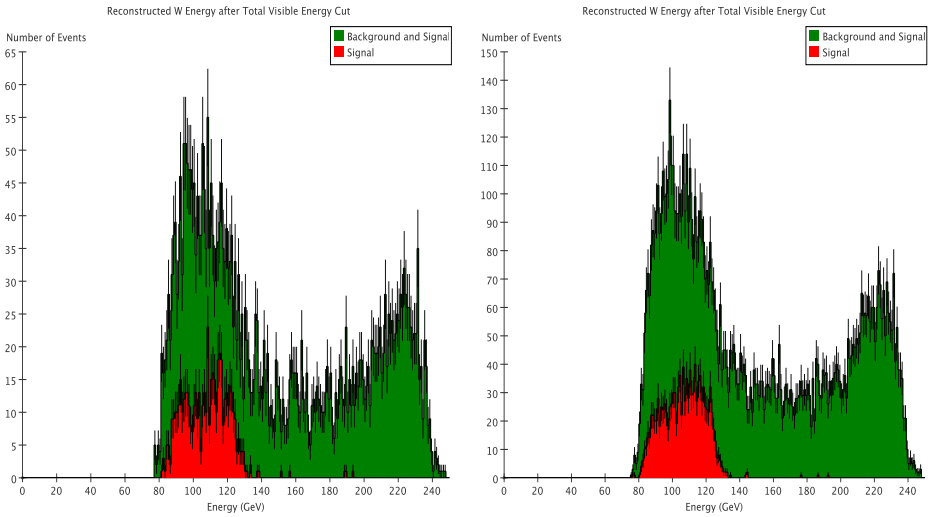

Figure 7: Reconstructed W Boson Energy at Point E' after Total Visible Energy Cut. The plot on the left is for 100 fb^{-1} of data and the one on the right is 250 fb^{-1} of data. This cut primarily has an effect at the higher energies and begins to remove the other peak.

W Boson Energy Cut

In a similar vein to the previous cut, the total energy of each W boson must be less than 175 GeV. It is slightly less restrictive in its assumption about the mass of the $\widetilde{\chi}_1^0$ than the previous cut because it only assumes that the $\widetilde{\chi}_1^0$ mass is greater than 75 GeV. However, the overall cut is more effective because if either W has more than 175 GeV of energy, the event is rejected. Additionally, this does not remove any of the SUSY signal.

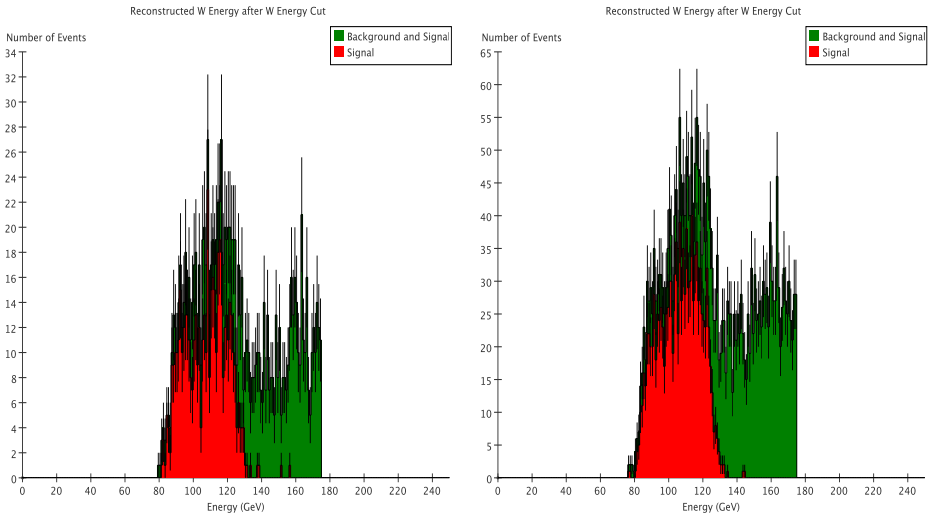

Figure 8: Reconstructed W Boson Energy at Point E' after W Boson Energy Cut. The plot on the left is for 100 fb^{-1} of data and the one on the right is 250 fb^{-1} of data. By removing the high energy particles, by conservation of energy they had to be paired with some lower energy particles. Therefore, this cut was quite important for decreasing the background at lower energies.

Angle Cut

The next cut that is applied to the data is a restriction on the angle of between the momentum of the two W bosons. The angle between W bosons in Standard Model events should be large if the event was reconstructed properly.

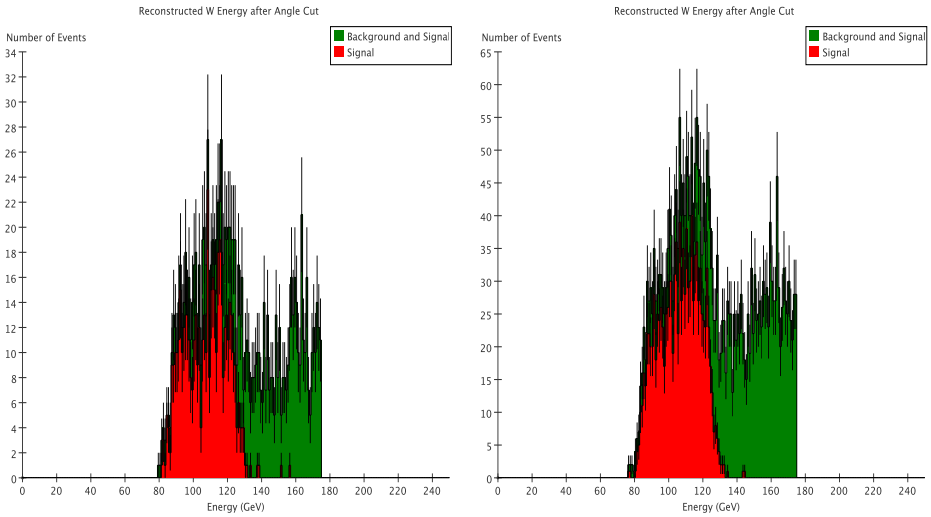

Figure 9: Reconstructed W Boson Energy at Point E' after Angle Cut. The plot on the left is for 100 fb^{-1} of data and the one on the right is 250 fb^{-1} of data. This cut did not remove many events, due to the fact that many of the events it would have removed have already been vetoed.

With these cuts final few cuts, the number of events removed is very small. This is partly due to the relatively small number of events.

Acoplanarity Cut

The final cut that will be applied is an acoplanarity cut. As detailed above, acoplanarity is the angle between the projection of the W boson momentum into the plane perpendicular to the beam axis. However, this cut is quite similar to the angle cut because both should be large for a Standard Model event.

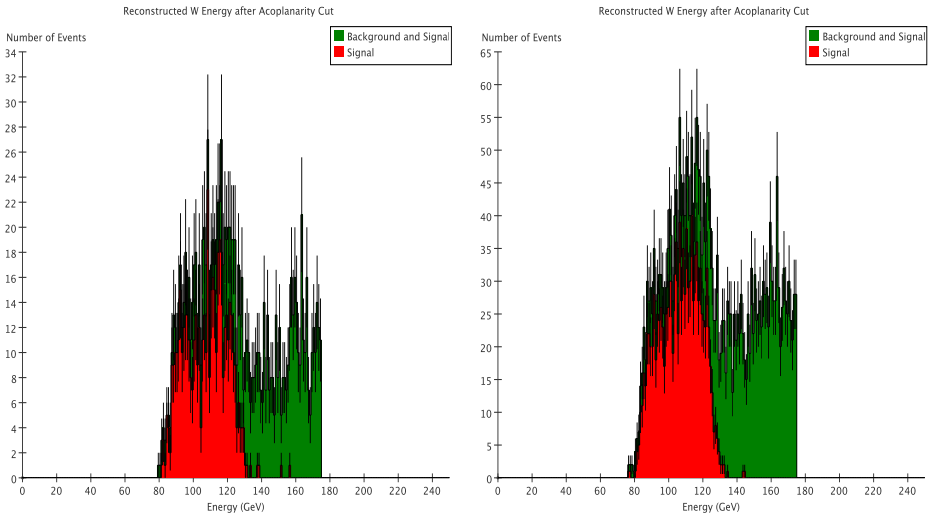

Figure 10: Reconstructed W Boson Energy at Point E' after Acoplanarity Cut. The plot on the left is for 100 fb^{-1} of data and the one on the right is 250 fb^{-1} of data. After all the cuts, the signal makes up a significant portion of the total number of events.

Applying all the cuts yields the following energy distributions which are reproduced for clarity. They have the same energy distribution as the plots for after the acoplanarity cut.

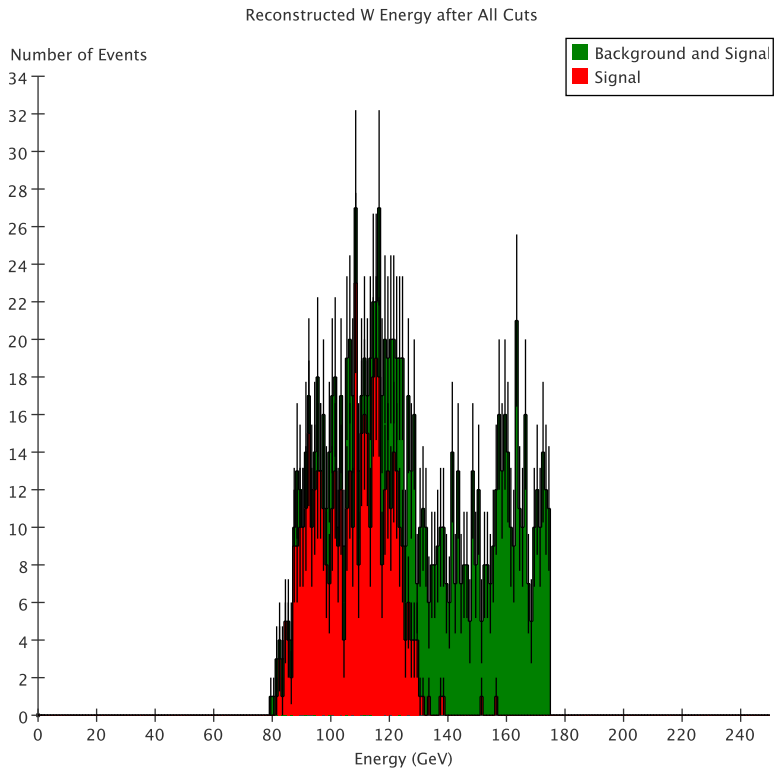

Figure 11: This plot shows the energy of the reconstructed W bosons with 100 fb^{-1} of data. The reconstructed signal by itself is superimposed in red onto both the background and signal combined.

The signal is visible over the constant Standard Model background, but the statistics are very low. As a result, a mass measurement is possible, but will not be very precise. To mitigate the problem with low statistics, the amount of data was increased to 250 fb^{-1}. This should increase the already visible features so that they can be measured. The increased data produces the following plot for the parameter point E'.

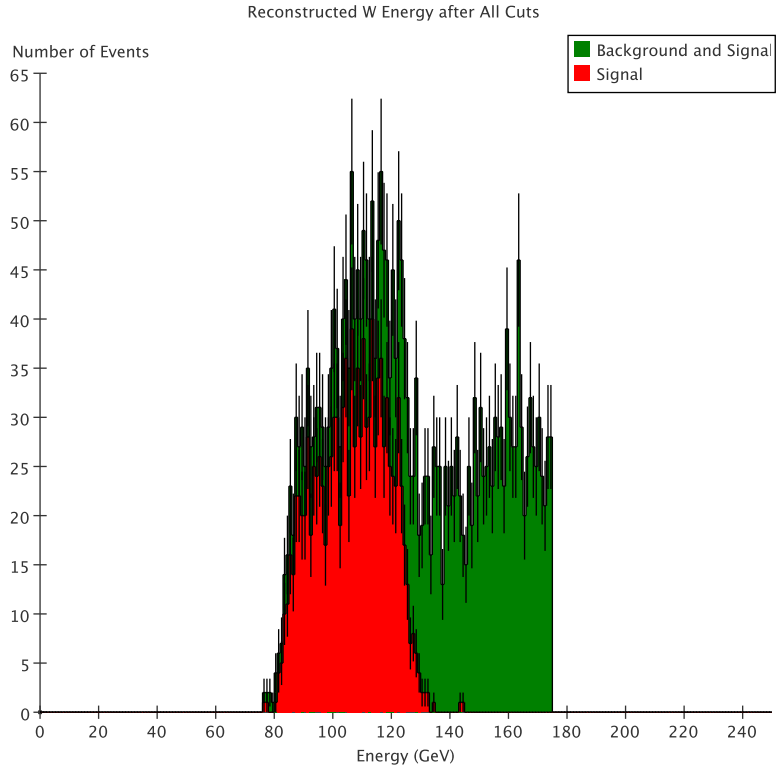

Figure 12: This plot shows the energy of the reconstructed W bosons with 250 fb^{-1} of data. The reconstructed signal by itself is superimposed in red onto both the background and signal combined. With the increased amount of data, the signal is quite visible. This will be analyzed to reconstruct the mass of the $\widetilde{\chi}_1^{\pm}$.

4 Mass Measurement

4.1 Endpoint Method

The first mass measurement technique used to extract the mass of the $\widetilde{\chi}_1^{\pm}$ is the endpoint method. First detailed in [14], a full derivation is provided in Appendix A. It relies on the relativistic kinematics of two-body decays to extract mass differences. From these mass differences, the mass of the $\widetilde{\chi}_1^{\pm}$ and the $\widetilde{\chi}_1^0$ can be extracted.

Calibration

The first step in making a mass measurement is to calibrate the measurement technique with the signal of interest. To do this, the Monte Carlo particles will be analyzed. The signal at 100 fb^{-1} and 250 fb^{-1} will be analyzed separately to find errors on each.

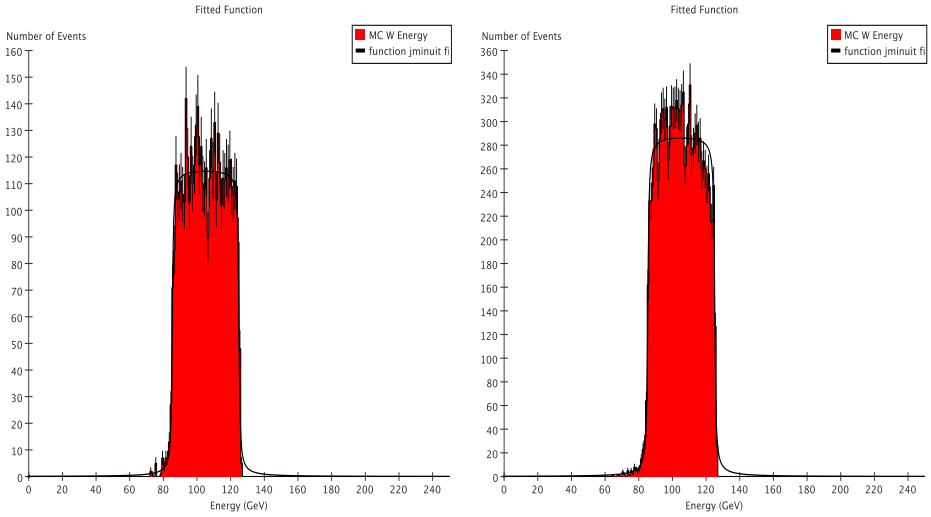

Figure 13: These plots show the fit of the Monte Carlo data. On the left is the 100 fb^{-1} plot while the 250 fb^{-1} plot is on the right. Both fits match the edges very closely. The mass from the left fit gives a mass of 237.0 GeV for the mass of the $\widetilde{\chi}_1^{\pm}$ and 124.0 GeV for the mass of the $\widetilde{\chi}_1^0$. For the right fit, the $\widetilde{\chi}_1^{\pm}$ mass is 237.0 GeV and the $\widetilde{\chi}_1^0$ mass is 123.7 GeV.

The actual mass of the $\widetilde{\chi}_1^{\pm}$ at the point E' is given above, and is 236.4 GeV. Similarly, the mass of the $\widetilde{\chi}_1^0$ is 123.3 GeV. The 100 fb^{-1} fit produces values of 237.0 GeV and 124.0 GeV for the mass of the $\widetilde{\chi}_1^{\pm}$ and $\widetilde{\chi}_1^0$, respectively. As a result, there is an error of 1 GeV on both of these measurements. For the 250 fb^{-1} fit, the results are similar. The measured masses are 237.0 GeV and 123.7 GeV. This implies that there is a discrepancy of 1 GeV for the $\widetilde{\chi}_1^{\pm}$ and a discrepancy of 0.5 GeV for the mass of the $\widetilde{\chi}_1^0$. Therefore, the increase in data does provide a slight improvement on the value of the masses.

Point E'

The Standard Model tail in both of the reconstructed plots for point E' presents a problem for this measurement technique. Because the fit function only has parameters for two edges, the fit will grab the wrong edge at 175 GeV, as seen below.

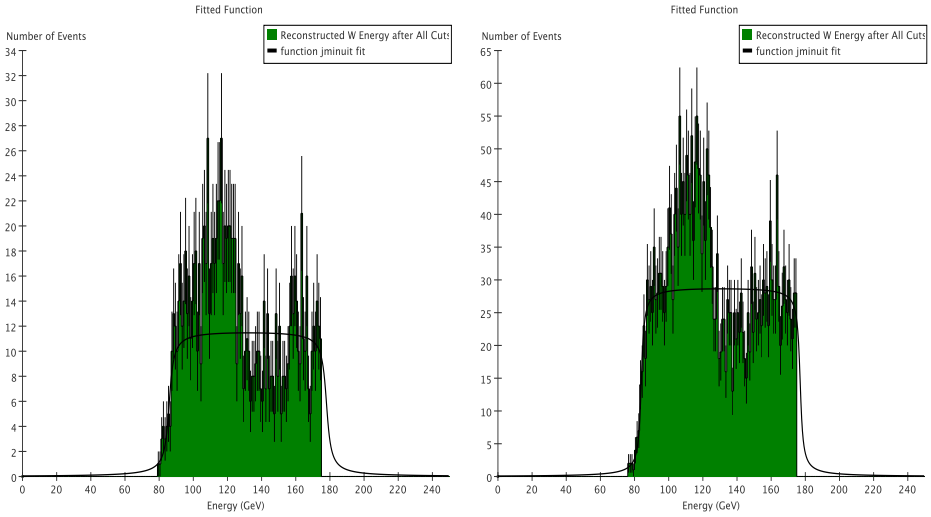

Figure 14: These plots show the fit of the reconstructed data. On the left is the 100 fb^{-1} plot while the 250 fb^{-1} plot is on the right. Due to the presence of the extra Standard Model background, the fit does not match the signal and fits to the wrong edge of the histogram.

To remedy this problem, the Standard Model background is examined. Since the Standard Model distribution is well known, a dataset can be simulated and then subjected to the cuts. Since the number of events is fairly small after applying all the cuts, the statistical errors that would have obscured the signal originally are reduced. Since the major background is from W boson pair production, this energy distribution will be subtracted from the full signal. This should isolate the low energy peak that clearly does not stem from a Standard Model process.

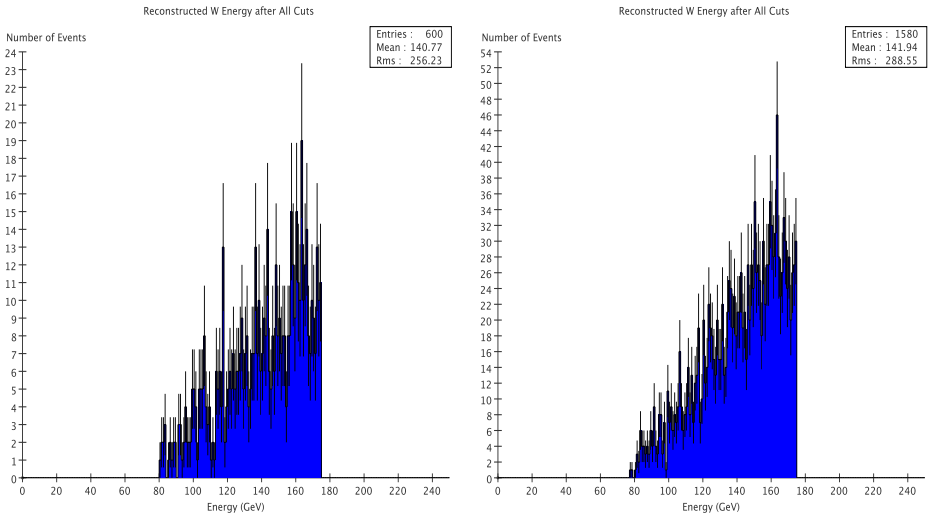

Figure 15: W Boson Pair Production Background after All Cuts. The Standard Model background has an exponentially decaying tail in this region, which demonstrates the prominence of the SUSY signal at the lower energies.

After removal of these background distributions, the signal distributions will be fitted once again. With the removal of the higher energy background processes, the SUSY signal is much more visible.

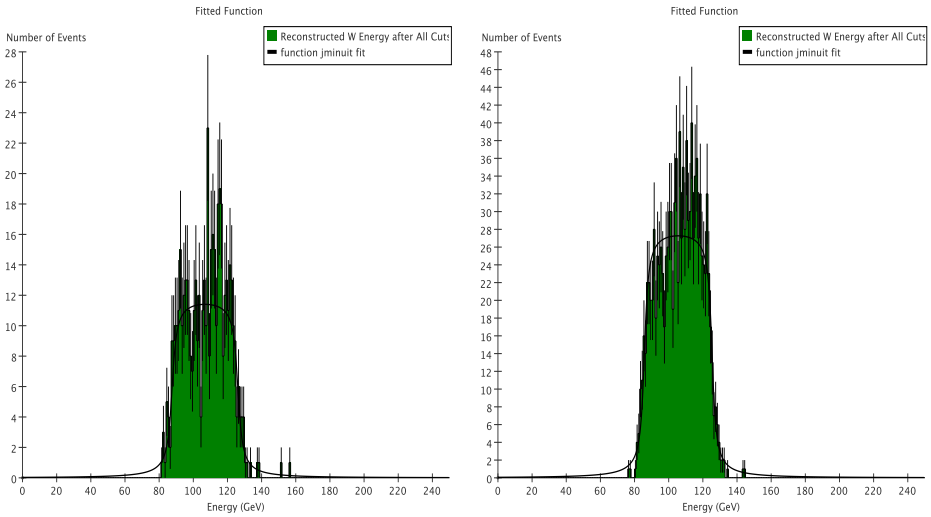

Figure 16: These plots show the fit of the reconstructed data. On the left is the 100 fb^{-1} plot while the 250 fb^{-1} plot is on the right. With the removal of the expected Standard Model background distribution, the SUSY signal is visible and able to fitted well. The 100 fb^{-1} fit on the left gives a $\widetilde{\chi}_1^{\pm}$ mass of 239.2 GeV and a $\widetilde{\chi}_1^0$ mass of 121.5 GeV. The 250 fb^{-1} fit gives masses of 237.4 GeV and 123.3 GeV for the $\widetilde{\chi}_1^{\pm}$ and $\widetilde{\chi}_1^0$, respectively.

The known mass of the $\widetilde{\chi}_1^{\pm}$ at point E' is 236.4 GeV and the known mass of the $\widetilde{\chi}_1^0$ is 123.3 GeV. The 100 fb^{-1} fit has a value of 239.2 GeV for the mass of the $\widetilde{\chi}_1^{\pm}$, so there is a discrepancy of 3 GeV to the known mass. Additionally, the mass of the $\widetilde{\chi}_1^0$ was measured to be 121.5 GeV, so this measurement has a discrepancy of 2 GeV. However, when the 250 fb^{-1} fit is considered, the measured masses improve considerably. The $\widetilde{\chi}_1^{\pm}$ mass is 237.4 GeV and the $\widetilde{\chi}_1^0$ mass is 123.3 GeV. Since there is a discrepancy of 1 GeV on the $\widetilde{\chi}_1^{\pm}$ mass and a discrepancy of 0.5 GeV on the $\widetilde{\chi}_1^0$ mass in the ideal case, as derived in the Calibration section, this is the uncertainty on these values. Consequently, both of the 250 fb^{-1} masses are consistent with the known masses. To verify that the cuts and removal of the expected Standard Model background did not disrupt the mass measurement, different techniques will also be investigated.

4.2 χ^2 Method

The next mass measurement technique that could be used is the χ^2 method. It is based upon the spectrum of the SUSY signal. A derivation is given in Appendix B, and is based upon the work of [15]. Additionally, [6] details the parameter point E' and shows the WMAP constraints on the parameter space. Due to the large nature of the m_0 parameter, the constraints are not plotted. Therefore, the valid regions over which the parameters could be varied are not known.

4.3 Threshold Scan

The final technique applied to this signal does not rely on the edges of the distribution. Instead, it seeks to find the center of mass energy where the process becomes kinematically accessible. By finding this point, the mass of the $\widetilde{\chi}_1^{\pm}$ can be calculated by dividing by two. This method has the advantage of not requiring a specific distribution or two-body decay. However, it relies on the assumption that the Standard Model background is constant over the range of the scan. The full derivation of the technique is provided in Appendix C. The particular implementation used here is a quartic polynomial.

Calibration

The calibration for this technique is somewhat different than for the endpoint method. For this method, the error is driven by the amount of data that is available to take. Since the SUSY cross sections are quite small, each energy in a given range will need to generate a large amount of data. Thus, the resolution is limited by the total amount of data that can be generated. To calibrate it, the assumption will be made that as much data as is necessary can be found. While this is not realistic, it provides a baseline, ideal case that can be compared to the others. For this run, the step size will be 1 GeV, with 100 fb^{-1} generated at each point from 450 GeV to 500 GeV.

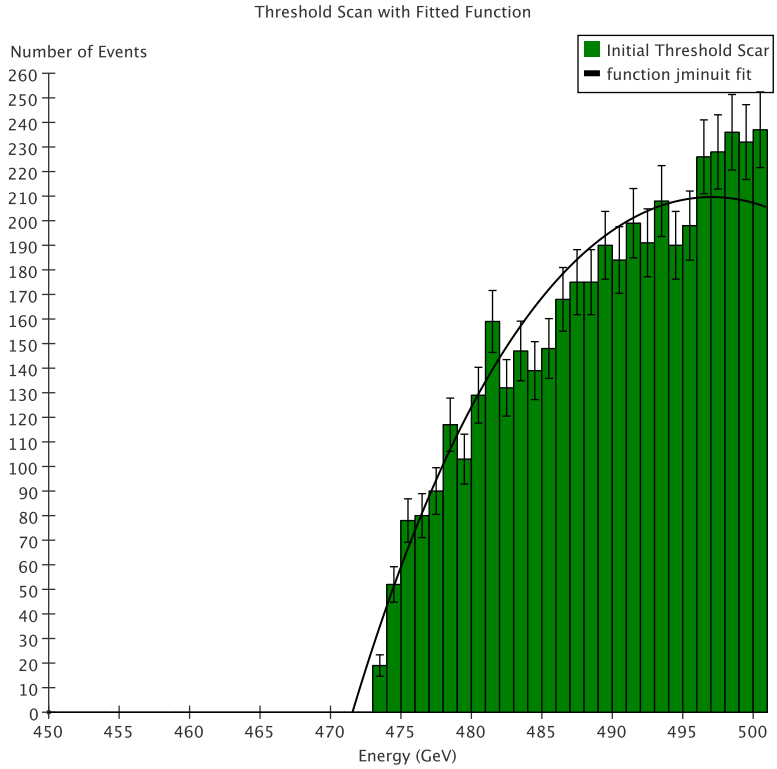

Figure 17: This plot shows the number of reconstructed events that pass the cuts detailed above. Since this is under the assumption of 100 fb^{-1} at at every step. The zero of this fit corresponds to a $\widetilde{\chi}_1^{\pm}$ mass of 236 GeV. Since the actual mass is 236.4 GeV, the minimum error on this method is determined by the step size. Therefore, the error on this measurement is 1 GeV.

Point E'

Even though the calibration was performed with as much data as needed, this is not a realistic assumption. Instead, the total amount of data will be limited to either 100 fb^{-1} or 250 fb^{-1}. With 100 fb^{-1} of data, the scan will be every 5 GeV with 10 fb^{-1} of data generated at each step. For 250 fb^{-1}, the step size will still be 5 GeV, but the amount of data will be increased to 25 fb^{-1} at each point.

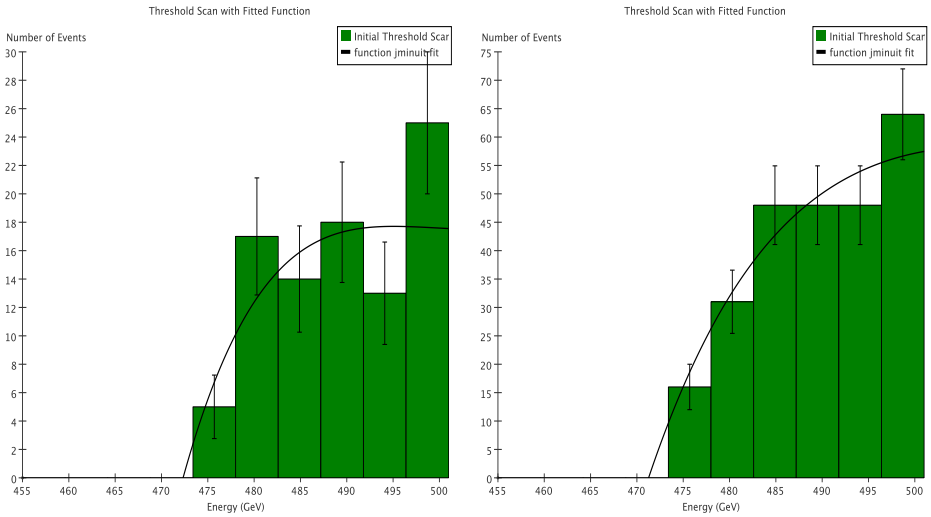

Figure 18: These plots show the fit of the reconstructed data using more realistic assumptions about the total amount of data available. On the left is the 100 fb^{-1} plot while the 250 fb^{-1} plot is on the right. The fit on the left produced a mass measurement of 236 GeV. The 250 fb^{-1} plot has a mass of 236 GeV. The error in both cases is at most 5 GeV since that is the step size.

Both mass measurements are consistent with the known $\widetilde{\chi}_1^{\pm}$ mass of 236.4 GeV. Additionally, the added statistics from increasing the dataset provides a much better measurement.

5 Conclusions

The hadronic $\widetilde{\chi}_1^{\pm}$ signal has been evaluated at all three kinematically accessible parameter points with a center of mass collision energy of 500 GeV. At points α and B' the number of hadronic events is too small to analyze the hadronic signal. However, at point E', it is possible to analyze the signal and extract a mass measurement. While it is not possible to find masses using the χ^2 method, both the threshold scan technique and the endpoint method are able to provide mass measurements. With the endpoint method, the measured mass of the $\widetilde{\chi}_1^{\pm}$ was 239 $\pm$ 1 GeV and 237 $\pm$ 1 GeV at 100 fb^{-1} and 250 fb^{-1}, respectively. Similarly, the $\widetilde{\chi}_1^0$ mass was measured to be 122

$\pm$ 1 GeV and 123.3 $\pm$ 0.5 GeV at 100 fb^{-1} and 250 fb^{-1}, respectively. The 250 fb^{-1} masses are consistent with the known values at point E' of 236.4 GeV for the $\widetilde{\chi}_1^{\pm}$ mass and 123.3 GeV for the $\widetilde{\chi}_1^0$ mass. Using the threshold scan technique, with 100 fb^{-1} of data, the measured mass of the $\widetilde{\chi}_1^{\pm}$ is 236 $\pm$ 5 GeV. With 250 fb^{-1} of data, the mass is 234 $\pm$ 5 GeV with much better statistics. Both of these are consistent with the true value of the $\widetilde{\chi}_1^{\pm}$ mass at point E': 236.4 GeV. One possible avenue for further study for the $\widetilde{\chi}_1^{\pm}$ is leptonic final states which have a larger cross section. However, under the proper conditions, it is possible to measure the mass of the $\widetilde{\chi}_1^{\pm}$ hadronically at the ILC.

Appendices

There are three primary techniques that can reconstruct the mass of a supersymmetric particle: the endpoint method [16] [14] [17], threshold scan method [18], and χ^2 method [15].

A Endpoint Method

The endpoint method is the conceptually simplest measurement technique and also the easiest to implement. However, this method can only be applied to two-body decays of the form:

$$A \rightarrow B + C$$

In this case the energy spectrum of either B or C is examined and should exhibit a shelf-like behavior as in the following plot. From this plot, the edges of the histogram can be extracted. This information leads to mass differences which allow for the determination of the other masses. If the edges of the energy spectrum of C are extracted from the fit and the mass of C is known, then the mass of both A and B can be found.

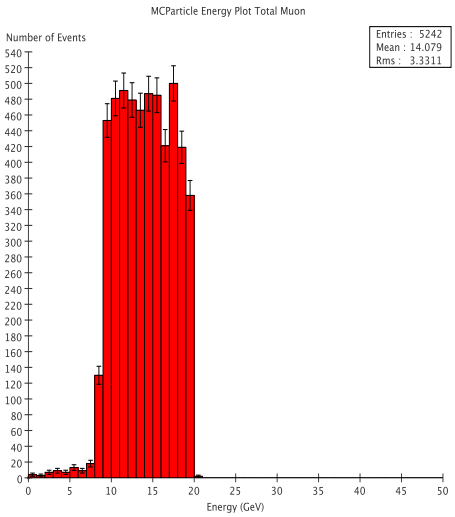

Figure 19: This plot shows the energy spectrum of the muons produced from the process $\widetilde{\mu}_R^{\pm} \rightarrow \mu^{\pm}\widetilde{\chi}_1^0$. This plot was created using MC particles to demonstrate the shelf-like behavior of a two-body decay.

A.1 Derivation

The following derivation is based on similar ones present in [14] and [17]. To begin with, a two-body decay of the form

$$A \rightarrow B + C$$

is assumed. For this derivation, the energy spectrum and mass of C will be known and the masses of A and B are to be determined. Now, let p_A, p_B, and p_C be the energy-momentum four vectors of A, B, and C, respectively. Then, due to conservation of energy and momentum,

$$p_A = p_B + p_C$$

$$p_B = p_A - p_C$$

This equation can be squared to yield

$$M_B^2 = M_C^2 + M_A^2 - 2p_A p_C \tag{4}$$

where the following identity has been used, in natural units, with the energy, E, and momentum vector, P:

$$p^2 = E^2 - P^2 = M^2 \tag{5}$$

In the center of mass frame of A, it has no momentum, so

$$p_A = M_A \tag{6}$$

Now, (6) can be substituted into (4) which can then be solved for p_C:

$$p_C = \frac{M_A^2 + M_C^2 - M_B^2}{2M_A} \tag{7}$$

Now since this analysis was conducted in the center of mass frame of A, this corresponds to a range in energies in the lab frame. Taking a Lorentz transformation yields:

$$E_{C,\,\mathrm{lab}} = \gamma(E_{C,\,\mathrm{cm}} - \beta P_{C,\,\mathrm{cm}} \cos\theta)$$

This equation leads to both a maximum and minimum possible energy which will be used to solve for the center of mass energy. Thus,

$$E_{\max} = \gamma(E_{C,\,\mathrm{cm}} + \beta P_{C,\,\mathrm{cm}}) \tag{8}$$

$$E_{\min} = \gamma(E_{C,\,\mathrm{cm}} - \beta P_{C,\,\mathrm{cm}}) \tag{9}$$

We can solve for $E_{C,\,\mathrm{cm}}$ by adding these equations together and simplifying.

$$E_{C,\,\mathrm{cm}} = \frac{E_{\max} + E_{\min}}{2\gamma} \tag{10}$$

Additionally, instead of adding (8) and (9), they can be multiplied to find

$$E_{\max}E_{\min} = \gamma^2(E_{C,\,\mathrm{cm}}^2 - \beta^2 P_{C,\,\mathrm{cm}}^2)$$

Now this can be simplified by using (5)

$$E_{\max}E_{\min} = \gamma^2(E_{C,\,\mathrm{cm}}^2 - \beta^2(E_{C,\,\mathrm{cm}}^2 - M_C^2))$$

$$E_{\max}E_{\min} = \gamma^2(1-\beta^2)E_{C,\,\mathrm{cm}}^2 + \gamma^2\beta^2 M_C^2 \tag{11}$$

Which can be simplified again because of the relationship between γ and β,

$$\gamma = \frac{1}{\sqrt{1-\beta^2}} \tag{12}$$

This implies that

$$E_{\max}E_{\min} = E_{C,\text{ cm}}^2 + \gamma^2\beta^2 M_C^2$$

Now, (10) will be substituted so that

$$E_{\max}E_{\min} = \frac{(E_{\max}+E_{\min})^2}{4\gamma^2} + \gamma^2\beta^2 M_C^2 \tag{13}$$

The final step is to solve for β and γ in terms of the desired quantities and then substitute. Therefore, from the definition,

$$\beta = \frac{P_{A,\text{ lab}}}{M_A} \tag{14}$$

Now, in the center of mass frame for A, $M_A = E_{A,\text{ cm}}$ since $P_{A,\text{ cm}} = 0$ from (5). Using this relation again gives

$$\beta = \frac{\sqrt{E_{A,\text{ cm}}^2 - M_A^2}}{E_{A,\text{ cm}}} \tag{15}$$

From this point, the denominator can be absorbed into the square root. Additionally, in the center of mass frame of the A pair, the particles being pair produced, each will have half the center of mass energy of the detector. This implies that:

$$E_{A,\text{ cm}} = \frac{\sqrt{s}}{2}$$

Therefore, (15) becomes

$$\beta = \sqrt{1 - \frac{4M_A^2}{s}} \tag{16}$$

Since β and γ are connected, this result can be applied to (12) to yield:

$$\gamma = \frac{\sqrt{s}}{2M_A} \tag{17}$$

Now, all relevant equations are in terms of the unknown mass, M_A, and known quantities. Therefore, (13), (16), and (17) are combined to find that

$$E_{\max}E_{\min} = \frac{(E_{\max}+E_{\min})^2}{4(s/4M_A^2)} + \frac{s}{4M_A^2}\left(1-\frac{4M_A^2}{s}\right)M_C^2$$

If both sides of this equation are multiplied by M_A^2, then it becomes a quadratic equation in M_A^2 which can be solved straightforwardly with the quadratic equation. Thus,

$$E_{\max}E_{\min}M_A^2 = \frac{(E_{\max}+E_{\min})^2}{s}M_A^4 + \frac{s}{4}\left(1-\frac{4M_A^2}{s}\right)M_C^2$$

which can be reduced to the familiar $ax^2+bx+c=0$ form:

$$\frac{(E_{\max}+E_{\min})^2}{s}M_A^4 - (E_{\max}E_{\min}+M_C^2)M_A^2 + \frac{sM_C^2}{4} = 0$$

Now, this implies that

$$M_A^2 = \frac{-b\pm\sqrt{b^2-4ac}}{2a} \tag{18}$$

where

$$a = \frac{(E_{\max}+E_{\min})^2}{s}$$
$$b = -(E_{\max}E_{\min}+M_C^2)$$
$$c = \frac{sM_C^2}{4}$$

Consequently, the discriminant in (18) can be simplified.

$$b^2-4ac = (E_{\max}E_{\min})^2 + 2E_{\max}E_{\min}M_C^2 + M_C^4 - (E_{\max}+E_{\min})^2M_C^2$$
$$b^2-4ac = M_C^4 - (E_{\max}^2+E_{\min}^2)M_C^2 + (E_{\max}E_{\min})^2$$
$$b^2-4ac = (M_C^2-E_{\max}^2)(M_C^2-E_{\min}^2) \tag{19}$$

Additionally, (19) can be substituted above to simplify (18)

$$\boxed{M_A^2 = \frac{E_{\max}E_{\min}+M_C^2\pm\sqrt{(M_C^2-E_{\max}^2)(M_C^2-E_{\min}^2)}}{2(E_{\max}+E_{\min})^2/s}} \tag{20}$$

From here it is straightforward to solve for M_A with the exception of the $\pm$ sign in front of the discriminant. When M_C is small and can be neglected, as in the case when plotting the energy spectrum of $e^{\pm}$ or $\mu^{\pm}$, the plus sign is appropriate. This follows from the fact that if we take the limit as $M_C \to 0$, (20) becomes

$$M_A^2 = \frac{E_{\max}E_{\min} \pm E_{\max}E_{\min}}{2(E_{\max} + E_{\min})^2/s} \tag{21}$$

Since the particle that is being reconstructed clearly does not have zero mass, the minus sign is disregarded to yield:

$$\boxed{M_A = \sqrt{s}\frac{\sqrt{E_{\max}E_{\min}}}{(E_{\max} + E_{\min})}} \tag{22}$$

which is the precise result derived in [14]. However, in the case where M_C is not negligible, such as reconstructing the $\widetilde{\chi}_1^{\pm}$ with $W^{\pm}$ bosons, the situation becomes more involved. In this case, the sign must be determined experimentally by looking for an energy, E_{crit}, where C is produced at rest in the lab. Then, for center of mass energies below this value, the particles are produced back to back and it is necessary to use the minus sign. However, if the energy is above the critical value, B and C will not be back to back, but instead travel in the same direction. In this case, the plus sign should be used. The easiest way to determine the critical value is through a threshold scan and will be discussed in the next appendix.

Once M_A has been determined, with the proper sign, M_B can be determined as well. Returning to (4), the known quantities can now be substituted so that, in the center of mass frame of A, the equation becomes

$$M_B^2 = M_C^2 + M_A^2 - 2M_A E_{C,\text{cm}}$$

Using (10) and (17) to substitute for $E_{C,\text{cm}}$,

$$M_B^2 = M_C^2 + M_A^2 - 2M_A\left(\frac{E_{\max} + E_{\min}}{2\sqrt{s}/2M_A}\right)$$

$$\boxed{M_B^2 = M_C^2 + M_A^2 - 2M_A^2\left(\frac{E_{\max} + E_{\min}}{\sqrt{s}}\right)} \tag{23}$$

This result agrees with the one derived in [17].

A.2 Error Analysis

Statistical Error

For both M_A and M_B, errors on the measured masses must be calculated. Returning to (20), and using the formula from [19],

$$\delta q = \sqrt{\left(\frac{\partial q}{\partial x}\delta x\right)^2 + \cdots + \left(\frac{\partial q}{\partial z}\delta z\right)^2} \tag{24}$$

Each partial derivative shall be calculated in turn using Mathematica. Along with the values from the fitted energy spectrum and their errors, this is enough to calculate the error on M_A and M_B. The derivation begins with a restatement of (20):

$$M_A = \sqrt{s}\sqrt{\frac{E_{\max}E_{\min} + M_C^2 \pm \sqrt{(M_C^2 - E_{\max}^2)(M_C^2 - E_{\min}^2)}}{2(E_{\max} + E_{\min})^2}}$$

In this instance, there are three independent variables, $E_{\max}$, $E_{\min}$, and M_C.

$$\frac{\partial M_A}{\partial E_{\max}} = \frac{\sqrt{s}\left(\frac{E_{\min}}{E_{\min}+E_{\max}} \pm \frac{E_{\max}}{E_{\min}+E_{\max}}\sqrt{\frac{M_C^2-E_{\min}^2}{M_C^2-E_{\max}^2}} - \frac{2\left(E_{\min}E_{\max}+M_C^2 \pm \sqrt{\left(M_C^2-E_{\min}^2\right)\left(M_C^2-E_{\max}^2\right)}\right)}{(E_{\min}+E_{\max})^2}\right)}{2\sqrt{2}\sqrt{E_{\min}E_{\max} + M_C^2 \pm \sqrt{\left(M_C^2 - E_{\min}^2\right)\left(M_C^2 - E_{\max}^2\right)}}}$$

$$\frac{\partial M_A}{\partial E_{\min}} = \frac{\sqrt{s}\left(\frac{E_{\max}}{E_{\max}+E_{\min}} \pm \frac{E_{\min}}{E_{\max}+E_{\min}}\sqrt{\frac{M_C^2-E_{\max}^2}{M_C^2-E_{\min}^2}} - \frac{2\left(E_{\max}E_{\min}+M_C^2 \pm \sqrt{\left(M_C^2-E_{\max}^2\right)\left(M_C^2-E_{\min}^2\right)}\right)}{(E_{\max}+E_{\min})^2}\right)}{2\sqrt{2}\sqrt{E_{\max}E_{\min} + M_C^2 \pm \sqrt{\left(M_C^2 - E_{\max}^2\right)\left(M_C^2 - E_{\min}^2\right)}}}$$

$$\frac{\partial M_A}{\partial M_C} = \frac{\sqrt{s}\left(2M_C \pm \frac{M_C\left(M_C^2-E_{\max}^2\right)+M_C\left(M_C^2-E_{\min}^2\right)}{\sqrt{\left(M_C^2-E_{\max}^2\right)\left(M_C^2-E_{\min}^2\right)}}\right)}{2\sqrt{2}(E_{\max} + E_{\min})\sqrt{E_{\max}E_{\min} + M_C^2 \pm \sqrt{\left(M_C^2 - E_{\max}^2\right)\left(M_C^2 - E_{\min}^2\right)}}}$$

Therefore, the statistical error on M_A is, with the above definitions:

$$\boxed{\delta M_A = \sqrt{\left(\frac{\partial M_A}{\partial E_{\max}}\delta E_{\max}\right)^2 + \left(\frac{\partial M_A}{\partial E_{\min}}\delta E_{\min}\right)^2 + \left(\frac{\partial M_A}{\partial M_C}\delta M_C\right)^2}} \tag{25}$$

Additionally, M_B is related to M_A through (23), which is restated:

$$M_B = \sqrt{M_C^2 + M_A^2 - 2M_A^2\left(\frac{E_{\max} + E_{\min}}{\sqrt{s}}\right)}$$

Consequently, there are 4 variables in this equation so the error becomes

$$\boxed{\delta M_B = \sqrt{\left(\frac{\partial M_B}{\partial E_{\max}}\delta E_{\max}\right)^2 + \left(\frac{\partial M_B}{\partial E_{\min}}\delta E_{\min}\right)^2 + \left(\frac{\partial M_B}{\partial M_C}\delta M_C\right)^2 + \left(\frac{\partial M_B}{\partial M_A}\delta M_A\right)^2}}$$

with the following definitions.

$$\frac{\partial M_B}{\partial E_{\max}} = -\frac{M_A^2}{\sqrt{-2\sqrt{s}M_A^2(E_{\max} + E_{\min}) + sM_A^2 + sM_C^2}}$$

$$\frac{\partial M_B}{\partial E_{\min}} = -\frac{M_A^2}{\sqrt{-2\sqrt{s}M_A^2(E_{\max} + E_{\min}) + sM_A^2 + sM_C^2}}$$

$$\frac{\partial M_B}{\partial M_C} = \frac{\sqrt[4]{s}M_C}{\sqrt{-2M_A^2(E_{\max} + E_{\min}) + \sqrt{s}M_A^2 + \sqrt{s}M_C^2}}$$

$$\frac{\partial M_B}{\partial M_A} = \frac{\sqrt{s}M_A - 2M_A(E_{\max} + E_{\min})}{\sqrt{-2\sqrt{s}M_A^2(E_{\max} + E_{\min}) + M_A^2 + M_C^2}}$$

Systematic Error

There is also systematic error introduced into this measurement as a result of the event generation process. These could be from initial state radiation, final state radiation, beamstrahlung, or detector simulation. However, with this measurement technique, it is possible to estimate the systematic error through the use of Monte Carlo data. Since this represents the best possible reconstruction, reconstructing the mass from this data and observing the discrepancy is the most realistic way to find the systematic error. However, this analysis should be repeated with the particular signal of interest and cannot be done in complete generality.

B χ^2 Method

B.1 Derivation

As detailed in [15], the χ^2 method is another technique for measuring the mass of supersymmetric particles. In this case, the spectrum of the decays products are examined. Then, for a given set of SUSY parameters, the spectrum is again calculated. These two spectrum histograms are compared bin by bin and the difference squared between them is tallied. When these are summed, it is the χ^2 value for that point. Then given a sufficient number of points, a minimum can be found which corresponds to the most likely SUSY parameter point. From this knowledge, the mass at the most likely parameter point is also the most likely value of the mass. Due to its dependence only on the spectrum of the decay products, and not the edges of the distribution, this method is particularly well suited for measuring the mass of many supersymmetric which do not decay through two-body decays. As such, it provides a natural complement to the endpoint method and is also useful for studying productions modes other than pair production.

B.2 Error Analysis

The error associated with this method can be extracted by finding the error on the minimum of the parabola associated with the χ^2 fit. Then, this error corresponds to a range of parameter values which give different masses. By examining the largest and smallest values this range can take, the error on the mass can be calculated. However, this error is dependent on the particular implementation of the fitting process.

Assumptions

The most problematic assumption about the χ^2 method is that it is quite heavily model dependent. For example, the spectrum differs greatly between the different formulations of SUSY, such as minimal super gravity, anomaly mediated supersymmetry breaking (AMSB), or gauge mediated supersymmetry breaking (GMSB). Consequently, if none of the currently researched theories accurately describe the underlying physics, this method will not provide significant or accurate results.

C Threshold Scan Method

The basis for this method is drawn from [18], where it is applied to W^+W^- studies. However, in this instance the method has been expanded to study supersymmetric particles. Additionally, it can be used to find E_{crit} as mentioned above in conjunction with the endpoint method.

The basic premise for this technique is that each process possesses a unique "turn-on point", or threshold point, below which production is not kinematically accessible. However, after this point, the cross section steadily increases. Therefore, as the center of mass energy is varied, the number of events should increase. Then, these results can be plotted and the zero fitted. This zero should correspond to when the process becomes kinematically accessible and is equal to the sum of the rest masses of the particles in the process.

C.1 Derivation

Known Mass in Pair Production

Typically, the threshold scan method will be applied to pair production because once the threshold point is determined, the mass of the particle can be determined easily by simply dividing the threshold energy by two. This can be accomplished in generality and is very useful for processes that do not undergo two-body decays, such as $\widetilde{\tau}_1^{\pm}$ production. However, if the particle decays through a two-body decay, then in a similar manner to the endpoint method, the mass of the other product can be determined as well. In particular, at E_{crit}, the measurable product is produced at rest in the lab. Consequently, the following decay will be considered:

$$e^+e^- \to A + A \quad \text{where} \quad A \to B + C$$

Under the assumption that M_A and M_B are known from the threshold point and E_{crit} is known, M_C will be found. Using the same convention for four-vectors as above in the endpoint method, in the lab frame this translates to

$$p_A = p_B + p_C$$

Now, this equation is squared and simplified using (5) and the fact that $P_B = 0$ in the lab frame since the energy is E_{crit}. This implies

$$M_A^2 = M_B^2 + M_C^2 + 2M_B E_C \tag{26}$$

Now, E_C is also equal to

$$E_C = \sqrt{M_C^2 + P_C^2} \tag{27}$$

But P_C is equal to P_A in the lab frame since momentum must be conserved and $P_B = 0$. Additionally, P_A is equal to

$$P_C = P_A = \sqrt{E_A^2 - M_A^2} \tag{28}$$

But, as before, $E_A = E_{\text{crit}}/2$ since only pair production is currently being considered. Combining (27) and (28) into (26), it follows that

$$M_A^2 - M_B^2 - M_C^2 = 2M_B\sqrt{M_C^2 - M_A^2 + \frac{E_{\text{crit}}^2}{4}}$$

The only unknown in this equation is M_C, so it can be solved to yield the desired mass. Squaring both sides,

$$(M_A^2 - M_B^2 - M_C^2)(M_A^2 - M_B^2 - M_C^2) = 4M_B^2\left(M_C^2 - M_A^2 + \frac{E_{\text{crit}}^2}{4}\right)$$

Expanding both sides and arranging like terms yields

$$M_C^4 + (-2M_B^2 - 2M_A^2)M_C^2 + (M_A^2 + M_B^2)^2 - M_B^2E_{\text{crit}}^2 = 0$$

This quartic can be solved by for M_C^2 using the quadratic equation. Thus,

$$M_C^2 = \frac{2M_B^2 + 2M_A^2 \pm \sqrt{(-2M_B^2 - 2M_A^2)^2 - 4(1)((M_A^2 + M_B^2)^2 - M_B^2E_{\text{crit}}^2)}}{2}$$

But the first two terms in the discriminant cancel and so this becomes

$$M_C^2 = \frac{2M_B^2 + 2M_A^2 \pm 2M_BE_{\text{crit}}}{2}$$

$$M_C = \sqrt{M_B^2 + M_A^2 \pm M_BE_{\text{crit}}}$$

Now, the sign must be taken to be minus because otherwise $M_C > M_A$ where C is a daughter particle of A. Since this would violate the conservation of energy, this is clearly not feasible. Therefore,

$$\boxed{M_C = \sqrt{M_B^2 + M_A^2 - M_BE_{\text{crit}}}} \tag{29}$$

Consequently, given M_A, M_B, and E_{crit} in a two-body decay, M_C can be found.

Unknown Mass in Pair Production

Additional information can be gleaned if M_B, E_{crit}, E_{min} and E_{max} are known. E_{crit} is defined as the place where the observable product of a two-body decay is produced at rest in the lab. This translates into a requirement that $E_{\text{min}} = M_B$, where M is the mass of the particle and E_{min} is the lower edge of the energy spectrum. If instead E_{max} is considered, then C will be produced at rest in the lab since this just corresponds to an inversion of the situation considered above. Now, consider E_A.

$$E_A = E_B + E_C$$

In this instance, $E_A = E_{\text{crit}}/2$ for pair production, $E_B = E_{\text{max}}$, and $E_C = M_C$ since it was produced at rest in the lab frame. Ergo,

$$\frac{E_{\text{crit}}}{2} = E_{\text{max}} + M_C$$

This implies that

$$\boxed{M_C = \frac{E_{\text{crit}}}{2} - E_{\text{max}}} \tag{30}$$

Now, M_A can be calculated as well. Using (5) in the lab frame,

$$E_A = \sqrt{M_A^2 + P_A^2}$$

But $P_A = P_B$ and the mass and energy of B are known. Therefore,

$$\frac{E_{\text{crit}}}{2} = \sqrt{M_A^2 + (E_{\text{max}}^2 - M_B^2)}$$

Solving this for M_A yields

$$\boxed{M_A = \sqrt{\frac{E_{\text{crit}}^2}{4} - E_{\text{max}}^2 + M_B^2}} \tag{31}$$

Other Applications

While typically used for pair production, a threshold scan can be used when considering general decays of the form

$$e^+e^- \rightarrow A + B$$

and a mass difference can be extracted from the turn-on point. In generality only the trivial mass difference

$$E_{\text{crit}} = M_A + M_B$$

can be extracted. However, when paired with another mass difference or an already known mass, this technique can provide valuable information.

C.2 Error Analysis

Known Mass in Pair Production

As was derived above in (32), M_C is found to be:

$$M_C = \sqrt{M_B^2 + M_A^2 - M_B E_{\text{crit}}} \tag{32}$$

Consequently, the error on this result can be propagated using (24). Therefore, the partial derivatives of M_C with respect to M_A, M_B, and E_{crit} will be calculated to yield:

$$\frac{\partial M_C}{\partial M_A} = \frac{M_A}{\sqrt{M_B^2 + M_A^2 - M_B E_{\text{crit}}}}$$

$$\frac{\partial M_C}{\partial M_B} = \frac{-M_B}{2\sqrt{M_B^2 + M_A^2 - M_B E_{\text{crit}}}}$$

$$\frac{\partial M_C}{\partial E_{\text{crit}}} = \frac{2M_B - E_{\text{crit}}}{2\sqrt{M_B^2 + M_A^2 - M_B E_{\text{crit}}}}$$

which can be combined in the following equation:

$$\boxed{\delta M_C = \sqrt{\left(\frac{\partial M_C}{\partial M_A}\delta M_A\right)^2 + \left(\frac{\partial M_C}{\partial M_B}\delta M_B\right)^2 + \left(\frac{\partial M_C}{\partial E_{\text{crit}}}\delta E_{\text{crit}}\right)^2}} \tag{33}$$

Unknown Mass in Pair Production

In the case that the mass of the particle being pair produced is unknown, then the analysis follows as above. Recalling from above (30), that M_C is given by:

$$M_C = \frac{E_{\text{crit}}}{2} - E_{\text{max}}$$

Consequently, the error on this measurement is given by:

$$\boxed{\delta M_C = \sqrt{\frac{1}{4}\delta E_{\text{crit}}^2 + \delta E_{\text{max}}^2}} \tag{34}$$

Additionally, from (31),

$$M_A = \sqrt{\frac{E_{\text{crit}}^2}{4} - E_{\text{max}}^2 + M_B^2}$$

Therefore, the error on this mass is given by:

$$\boxed{\delta M_A = \sqrt{\left(\frac{\partial M_A}{\partial E_{\text{crit}}}\delta E_{\text{crit}}\right)^2 + \left(\frac{\partial M_A}{\partial E_{\text{max}}}\delta E_{\text{max}}\right)^2 + \left(\frac{\partial M_A}{\partial M_B}\delta M_B\right)^2}} \tag{35}$$

where each partial derivative is given by the following.

$$\frac{\partial M_A}{\partial E_{\text{crit}}} = \frac{E_{\text{crit}}}{4\sqrt{\frac{1}{4}E_{\text{crit}}^2 - E_{\text{max}}^2 + M_B^2}}$$

$$\frac{\partial M_A}{\partial E_{\text{max}}} = \frac{-E_{\text{max}}}{\sqrt{\frac{1}{4}E_{\text{crit}}^2 - E_{\text{max}}^2 + M_B^2}}$$

$$\frac{\partial M_A}{\partial M_B} = \frac{M_B}{\sqrt{\frac{1}{4}E_{\text{crit}}^2 - E_{\text{max}}^2 + M_B^2}}$$

Assumptions

While this method is more robust than the endpoint method in that it doesn't depend critically upon edges of a distribution, there is one major assumption that must be accounted for to successfully apply this method. In particular, since the entire background cannot be generated at each discrete energy due to computational limitations, the background is assumed to be constant over the range of energies considered. Consequently, the range for the threshold scan cannot be too large or this assumption is bound to fail. However, the assumption of constant background will be investigated more closely through examination of Standard Model cross sections.

Standard Model Cross Sections

To more thoroughly evaluate the assumption of relatively constant Standard Model background, plots of cross section versus energy will be constructed for many Standard Model processes.

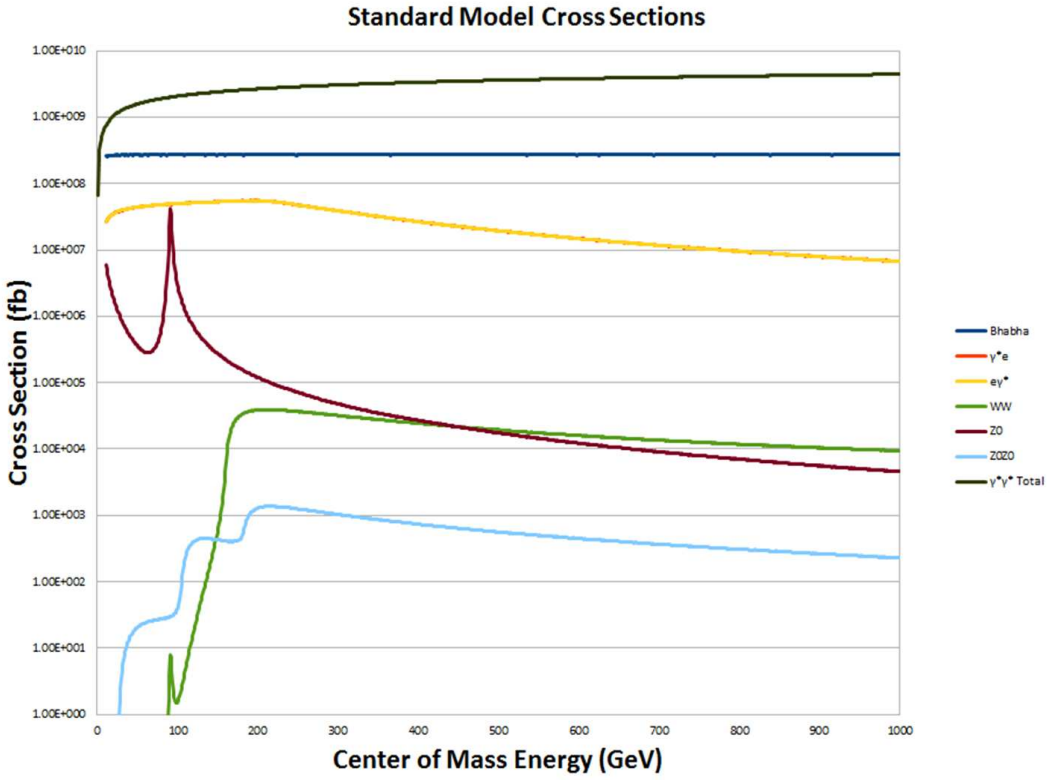

Figure 20: This plot shows how several important Standard Model background process cross sections vary with the center of mass energy of the detector. As can be seen above, over a small range, the assumptions made for the threshold scan method do hold. However, over large ranges this method should be used very carefully. Additionally, the eγ* and γ*e have the same cross section and so only one line is visible.

References

[1] S. Martin. A Supersymmetry Primer. 2006. arXiv: hep-ph/9709356.

[2] ILC Home. http://www.linearcollider.org/cms/.

[3] SiD Home. http://silicondetector.org/display/SiD/home.

[4] ILD Home. http://www.ilcild.org/.

[5] M. Battaglia et al. Physics Benchmarks for the ILC Detectors. 2006. arXiv: hep-ex/0603010.

[6] M. Battaglia et.al. Updated Post-WMAP Benchmarks for Supersymmetry. 2003. arXiv: hep-ph/0306219v1.

[7] Comput. Phys. Commun. 153 (2003) 275. arXiv:hep-ph/0301101.

[8] N. Metropolis. Beginning of the Monte Carlo Method. 1987. http://library.lanl.gov/la-pubs/00326866.pdf.

[9] JHEP 05 (2006) 026. arXiv:hep-ph/0603175.

[10] P.H. Daverveldt F.A. Berends and R. Kleiss. Monte carlo simulation of two-photon processes. *Comp. Phys. Commun.*, 1986.

[11] org.lcsim home. http://confluence.slac.stanford.edu/display/ilc/org.lcsim.

[12] G. Oleinik et. al. Electron Detection Efficiency of the SiD02 Beam Calorimter. 2009. http://hep-www.colorado.edu/~uriel/Beamstrahl_TwoPhoton-Process/grp_results.html.

[13] Carola F. Berger, James S. Gainer, JoAnne L. Hewett, Ben Lillie, and Thomas G. Rizzo. General Features of Supersymmetric Signals at the ILC: Solving the LHC Inverse Problem. 2007. arXiv: hep-ph/0712.2965.

[14] Elizabeth Goodman. The Search for the Supersymmetric Selectron. http://hep-www.colorado.edu/SUSY/grpwk_anal.html.

[15] Andrew Hahn. An Analysis of Selectron Masses Including the Effects of Beamstrahlung. hep-www.colorado.edu/SUSY/grpwk_anal.html.

[16] Nick Danielson. Determining the Mass of the Snuetrino and Chargino By Examining the Snuetrino Sneutrino Production Mode. `hep-www.colorado.edu/SUSY/grpwk_anal.html`.

[17] Brook Williams. Study of the Production of Supersymmetric Particles. `hep-www.colorado.edu/SUSY/grpwk_anal.html`.

[18] M. Boonekamp et. al. Threshold Scan in Diffractive W Pair Production via QED Processes at the LHC. 2007. arXiv: hep-ph/0709.2742.

[19] John R. Taylor. *An Introduction to Error Analysis*. University Science Books.